Counting function for a sphere of anisotropic quartz

Niels Søndergaard,[1,*] Thomas Guhr,[1,†] Mark Oxborrow,[2,‡] Kristian Schaadt,[3,§] and Clive Ellegaard[3,‖]
[1]*Matematisk Fysik, LTH, Lunds Universitet, Sweden*
[2]*National Physics Laboratory, Teddington, United Kingdom*
[3]*Niels Bohr Institute, Copenhagen, Denmark*
(Received 17 October 2003; revised manuscript received 12 May 2004; published 15 September 2004)

We calculate the leading Weyl term of the counting function for a monocrystalline quartz sphere. In contrast to other studies of counting functions, the anisotropy of quartz is a crucial element in our investigation. Hence we do not obtain a simple analytical form, but we carry out a numerical evaluation. To this end we employ the Radon transform representation of the Green's function. We compare our result to a previously measured unique data set of several tens of thousands of resonances.

DOI: 10.1103/PhysRevE.70.036206 PACS number(s): 05.45.Mt, 43.20.+g, 43.40.+s

I. INTRODUCTION

In solid state physics [1], quantum chaos [2–5], and other applications a smooth approximation to the level density or, equivalently, to its integral referred to as the counting function (or staircase function) is often needed. Typically such an approximation is obtained by semiclassical methods [6]. Alternatively, related techniques stemming from geometrical quantization and index theorems [7] are occasionally employed. In the context of quantum chaos, this problem of counting the number of states has been studied thoroughly for finite systems, in particular, billiards. The latter are realized in microwave resonators. Quantum chaos methods were successfully applied to elastodynamical systems [8–15]. The semiclassical limit corresponds to a ray limit in which the wavelengths are much smaller than characteristic length scales of the resonating device. However, anisotropy enters as an important feature of these systems which is not present in scalar Schrödinger quantum mechanics. The problem of anisotropy also shows up in the calculation of the heat capacity in solid state physics which directly relates to the counting function.

In this contribution, we study a monocrystalline quartz sphere. We calculate the first approximation to the counting function which is referred to as the Weyl term in semiclassics. We combine analytical with numerical computations. Furthermore, we have a unique data set at our disposal which was measured previously with extraordinary resolution [16]. It comprises tens of thousands of resonances, enabling a comparison with our theoretical findings.

Even though the particular shape of a sphere was chosen the system will not be rotationally invariant due to the underlying medium, α quartz, which is anisotropic. This anisotropy leads to nonseparabillity of the wave equation. This makes the problem so complex that there is no way of calculating spectra other than by brute force numerical methods.

A major motivation for the present investigation is the renewed interest in elastomechanical problems which are increasingly important for microelectromechanical systems (MEMS's). In particular, a better understanding of spectral properties is expected to improve the control of the resonance and scattering pole structure of MEMS's. This in turn would allow the designing of better filters and actuators [17]. Thus deeper insight into the role of anisotropy is called for.

The paper is organized as follows. In Sec. II, we compile general features of elastodynamics as needed in the present context. We work out the Green's function in Sec. III. The data accumulation is briefly reviewed in Sec. IV; we compare to the experimental findings in Sec. V. We summarize and conclude in Sec. VI.

II. ELASTODYNAMICS

In Sec. II A, we sketch some properties of elastic waves in anisotropic materials. We discuss the dispersion relation and the slowness surfaces in Sec. II B. The Green's function is worked out in Sec. II C. The Einstein summation convention is assumed throughout.

A. Elastic wave equation

In linear elastodynamics in the time domain, the wave equation reads [18,19]

$$c_{ijkl}\frac{\partial^2 u_l}{\partial x_j\,\partial x_k}=\rho\frac{\partial^2 u_i}{\partial t^2}, \tag{1}$$

where the displacement field u_i describes the increment of a fictitious point particle at its position (x_1,x_2,x_3). The quantities c_{ijkl} form the elasticity tensor and ρ is the mass density. For our system, we may assume homogeneity of the material, that is, the mass density and the elasticity tensor are constants. In an isotropic material, the elasticity tensor has only two independent entries which yield, together with the mass density, the longitudinal velocity for pressure waves and the transverse velocity for shear waves. In our case of anisotropic quartz, the velocity of an elastic wave also depends on the direction in the crystal. This means that the

*Electronic address: Niels.Sondergaard@matfys.lth.se
†Electronic address: Thomas.Guhr@matfys.lth.se
‡Electronic address: Mark.Oxborrow@npl.co.uk
§Electronic address: Schaadt@nbi.dk
‖Electronic address: Ellegaard@nbi.dk

elasticity tensor has six independent entries. The elasticity tensor always fulfills the following symmetry conditions:

$$c_{ijkl} = c_{ijlk} = c_{klij}. \tag{2}$$

The wave equation (1) is valid in the regime where the linear relation

$$\sigma_{ij} = c_{ijkl} u_{kl} \tag{3}$$

holds between the stress tensor σ_{ij} and the strain tensor

$$u_{kl} = \frac{1}{2}\left(\frac{\partial u_k}{\partial x_l} + \frac{\partial u_l}{\partial x_k}\right). \tag{4}$$

Equation (3) is the most general form of Hooke's law. The wave equation in the frequency domain which corresponds to Eq. (1) reads

$$c_{ijkl}\frac{\partial^2 u_l}{\partial x_j \partial x_k} + \rho\omega^2 u_i = 0, \tag{5}$$

where the angular velocity is denoted ω.

We are interested in the elastic vibrations of a finite object, the elastic resonator, which is confined by a surface. Matching the situation in the experiment we assume free boundary conditions, that is, there is no normal stress on the surface. This is equivalent to the condition

$$0 = c_{ijkl} u_{kl} n_j \tag{6}$$

with the strain (4) and normal vector n_j. The boundary condition (6) is of Neumann type and makes it possible to mode convert at the boundary. In an isotropic material, a longitudinal (transverse) wave hitting the boundary is reflected and generates, apart from some special situations, a second wave which is transverse (longitudinal). These waves have different velocities and leave the point of incident under different angles. This formally corresponds to quantum mechanics for a free spin-one particle whose effective mass depends on the spin degrees of freedom. The particle is confined in an enclosure, corresponding to the resonator. Not surprisingly, mode conversion shows a much richer phenomenology in an anisotropic material.

B. Dispersion relation and slowness

We consider a plane wave with wave vector k_j, angular velocity ω, and polarization vector p_l,

$$u_l^{(\mathrm{pw})}(x_1,x_2,x_3) = p_l \exp(ik_j x_j - i\omega t). \tag{7}$$

Inserting this into the wave equation (1) yields the dispersion relations

$$c_{ijkl} k_j k_k p_l = \rho\omega^2 \delta_{il} p_l. \tag{8}$$

(Here k_j and k_k are the jth and the kth component, respectively, of the wave vector.) The wave numbers and the angular velocity occur in equal powers. This is exploited by considering their ratio, the *slowness* [20]

$$s_i = k_i/\omega. \tag{9}$$

The dispersion relations (8) then motivate the introduction of the matrix

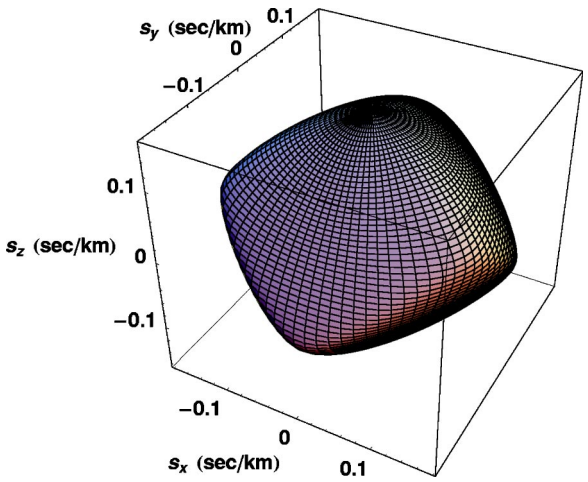

FIG. 1. (Color online) Quasilongitudinal slowness.

$$S_{il} = -\frac{1}{\rho} c_{ijkl} s_j s_k + \delta_{il}. \tag{10}$$

Thus Eq. (8) can be cast into the form $S_{il}p_l = 0$. For solutions to exist, one must have

$$\det \mathbf{S} = 0. \tag{11}$$

This defines the *slowness surface*. As each entry in Eq. (10) that is quadratic, the full determinantal condition becomes a polynomial of order 6 in the variables s_i. This condition gives rise to a surface depicted in Figs. 1–3. The elastic constants c_{ijkl} for quartz have been used; see Sec. V. The slowness coordinates are, except for a constant factor, coordinates in the space dual to the configuration space of the resonator. The units in the figures are in inverse velocities corresponding to velocities of the order 5000 m/sec. The surface consists of three sheets, $\Sigma = \cup_{\alpha=1}^{3} \Sigma_\alpha$, where only the inner one is convex. One clearly sees the D_3 symmetry of the crystal, that is, after a rotation of $2\pi/6$ around the symmetry axis a reflection in the plane orthogonal to the axis transforms the surface into itself. This surface is the remains of the dispersion surface after the frequency has been scaled

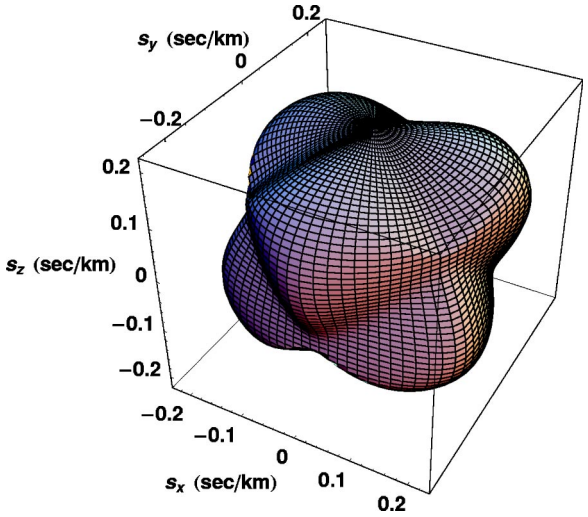

FIG. 2. (Color online) Quasitransverse 1 slowness.

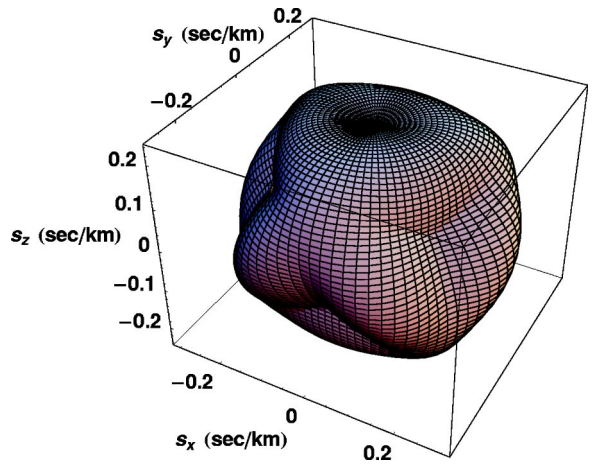

FIG. 3. (Color online) Quasitransverse 2 slowness.

out. Thus a fixed direction corresponds in general to three points on the slowness surface. The inner sheet is associated to an almost longitudinal polarization whereas the outer sheets are associated with the transverse polarization. Hence the terms quasilongitudinal and quasitransverse are used.

As already pointed out, our elastodynamical problem has formally much in common with quantum mechanics for a particle with spin confined to an enclosure, which could be viewed as a billiard. Inside the billiard, the particle moves in straight lines and it mode converts upon reflections at the boundaries. This is the situation in configuration space. Employing slowness, we have mapped the problem of one spherical billiard for a particle with spin onto the problem of a particle without spin (in a dual space) simultaneously moving in three nonspherical billiards, that is, in the spaces confined by the three slowness surfaces. A trajectory in configuration space consists of a sequence of straight pieces with a certain modal character. In slowness space, the particle jumpes between the billiards which are specific for a given modal character.

C. Group velocity and polarization

The Green's function to be introduced later on is a matrix due to the vector character of the elastic field. Thus it is useful to work with a proper basis in matrix space. Such a basis is formed by the projectors $\mathbf{e}_\alpha$ for a given polarization α. We shall consider the case where wave vectors belong to a fixed sheet of polarization α and discuss the associated group velocity. Below we denote polarization indices with Greek letters whereas geometrical indices are in *Roman* letters.

A projector $\mathbf{e}_\alpha$ is a 3×3 matrix which we introduce, corresponding to Eqs. (8) and (10), by writing

$$\mathbf{k}_\alpha \cdot \mathbf{c}/\rho \cdot \mathbf{k}_\alpha = \omega^2 \mathbf{e}_\alpha, \tag{12}$$

that is, $c_{pqrs}/\rho k_{\alpha,p} k_{\alpha,s} = \omega^2 e_{\alpha,qr}$. Each projector corresponds to one of the three possible polarizations α. The projectors $\mathbf{e}_\alpha$ satisfy the completeness relation

$$\sum_\alpha \mathbf{e}_\alpha = \mathbf{1}_{3\times 3} \tag{13}$$

and the relation

$$\mathbf{e}_\alpha \cdot \mathbf{e}_\beta = \delta_{\alpha\beta} \mathbf{e}_\alpha, \tag{14}$$

where the dot indicates matrix multiplication. The dispersion relation for a fixed polarization becomes

$$(\mathbf{k}_\alpha \cdot \mathbf{c}/\rho \cdot \mathbf{k}_\alpha) : \mathbf{e}_\alpha - \omega^2 = \mathbf{0}, \tag{15}$$

where the contraction of all indices is denoted by the : sign.

A natural quantity that now enters the discussion is the group velocity for a given polarization α,

$$\mathbf{v}_{g,\alpha} = \frac{\partial \omega}{\partial \mathbf{k}_\alpha}, \tag{16}$$

describing the change of angular velocity with the wave vector for that polarization. Varying Eq. (15) with respect to the wave vectors and the angular velocity

$$(d\mathbf{k}_\alpha \cdot \mathbf{c}/\rho \cdot \mathbf{k}_\alpha) : \mathbf{e}_\alpha - d\omega\omega = \mathbf{0} \tag{17}$$

and finally scaling out the angular velocity gives

$$\mathbf{v}_{g,\alpha} = \frac{\partial \omega}{\partial \mathbf{k}_\alpha} = (\mathbf{c}/\rho \cdot \mathbf{s}_\alpha) : \mathbf{e}_\alpha. \tag{18}$$

Above, also the projectors could have a variation which we have not taken into account. However, since

$$(\mathbf{k}_\alpha \cdot \mathbf{c}/\rho \cdot \mathbf{k}_\alpha) : d\mathbf{e}_\alpha = \omega^2 \mathbf{e}_\alpha : d\mathbf{e}_\alpha \tag{19}$$

and

$$2\mathbf{e}_\alpha : d\mathbf{e}_\alpha = d(\mathrm{tr}(\mathbf{e}_\alpha \cdot \mathbf{e}_\alpha)) = d(\mathrm{tr}(\mathbf{e}_\alpha)) = d(1) = 0, \tag{20}$$

this variation does not contribute.

From Eqs. (9) and (15) we see that $\mathbf{s}_\alpha$ and $\mathbf{v}_{g,\alpha}$ are mutually *polar reciprocal* to each other, that is,

$$1 = (\mathbf{s}_\alpha \cdot \mathbf{c}/\rho \cdot \mathbf{s}_\alpha) : \mathbf{e}_\alpha = \mathbf{s}_\alpha \cdot (\mathbf{c}/\rho \cdot \mathbf{s}_\alpha) : \mathbf{e}_\alpha = \mathbf{s}_\alpha \cdot \mathbf{v}_{\mathbf{g},\alpha}. \tag{21}$$

This relation can be used to construct the group velocity and holds in general for systems which are homogeneous in k_i and ω. This condition defines the individual sheet, and in particular the group velocity is normal to this sheet.

However, interesting complications arise as the degeneracy of this matrix is not constant. Hence there exist directions for which the phase velocity of the two intersecting sheets is the same. Note that this degeneracy occurs in slowness space. Interestingly such *mode conversion points* may also occur purely in x space, e.g., in Landau-Zener problems or in nuclear/chemical reaction physics. In general, however, there are three distinct polarizations, and from Eq. (10) these only depend on the direction $\hat{\mathbf{s}}_\alpha = \mathbf{s}_\alpha / s_\alpha$. Furthermore, for the opposite direction the same polarization is found. We have depicted one of the quasitransverse polarizations in Figs. 4 and 5. The behavior of the two shear components are similar with a twisting near the poles. The quasilongitudinal, however, is much simpler with a polarization vector which looks like a smooth deformation of the field of normal vectors on the sphere (a hedgehog); see Fig. 6.

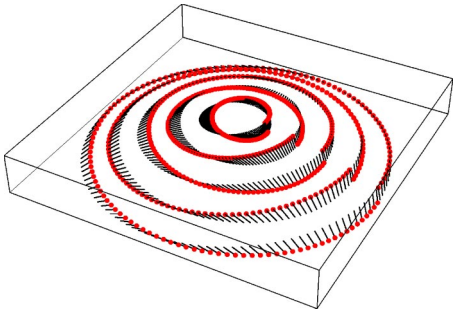

FIG. 4. (Color online) Twisting of polarization: shear 1.

III. GREEN'S FUNCTION

We discuss a result based on the Radon transform. Numerically it is convenient to express the Green's function as a certain integral over the unit sphere. For a theoretical interpretation this integral is transformed to a similar one over the slowness surface. Using the Radon transform the result in the frequency domain is [21,22]

$$\mathbf{G}_+(\mathbf{x},\omega) = \mathbf{G}_+^R(\mathbf{x},\omega) + \mathbf{G}^S(\mathbf{x},\omega) \tag{22}$$

with superscripts R and S indicating the *regular* and *singular* part and subscript + for *causal*. Here we have changed dimensions compared to Refs. [21,22] by solving for the Green's function for Eq. 5 where ρ has been divided out. For convenience a derivation is discussed in Appendix A. The regular part is an integral over plane waves:

$$\mathbf{G}_+^R(\mathbf{x},\omega) = \frac{\mathbf{i}}{8\pi^2}\int_{\mathbf{n}\in\mathbf{S}^2}\sum_\alpha \frac{k_\alpha \mathbf{e}^\alpha}{2c_\alpha^2} e^{ik_\alpha|\mathbf{n}\cdot\mathbf{x}|} d\Omega. \tag{23}$$

Here k_α, c_α, and $\mathbf{e}^\alpha$ refer to wave number, phase velocity, and respective polarization projector for polarization number α for the plane wave in question. The singular part

$$\mathbf{G}^S(\mathbf{x},\omega) = \frac{1}{8\pi^2}\int_{\mathbf{n}\in S^2} \mathbf{\Gamma}^{-1}(\mathbf{n})\,\delta(\mathbf{n}\cdot\mathbf{x})\,d\Omega \tag{24}$$

is purely real and corresponds to the *static* part of the Green's function. The matrix Γ is defined by

$$\Gamma_{ij} = \frac{c_{iklj}}{\rho} n_k n_l \tag{25}$$

for which

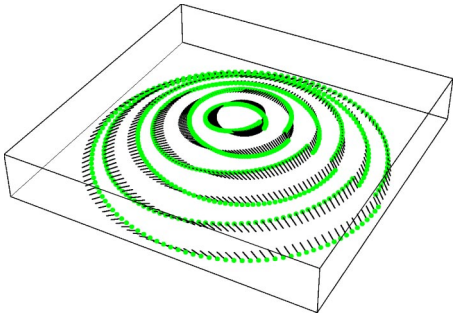

FIG. 5. (Color online) Twisting of polarization: shear 2.

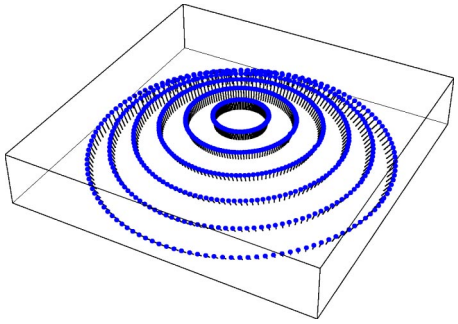

FIG. 6. (Color online) Polarization: pressure.

$$\mathbf{\Gamma}(\mathbf{n}) = \sum_\alpha c_\alpha^2 \mathbf{e}^\alpha. \tag{26}$$

We notice that Eq. (25) follows from Eq. (15) with $\mathbf{k}=\mathbf{n}k$ and $c=\omega/k$.

The integrals above can be formulated in a more intrinsic form. Thus instead of integrating over the unit sphere S^2 the dispersion surface can be applied. Using *slowness*, Eq. (23) becomes

$$\mathbf{G}_+^R(\mathbf{x},\omega) = \frac{i}{8\pi^2}\omega\int_{\mathbf{n}\in S^2}\sum_\alpha \frac{s_\alpha^3 \mathbf{e}^\alpha}{2} \mathbf{e}^{i\omega|\mathbf{s}_\alpha\cdot\mathbf{x}|} d\Omega. \tag{27}$$

Since the wave number and the angular velocity occur homogeneously in the dispersion relation the corresponding slowness surface is used. Applying polar reciprocity (21), $1=\mathbf{s}\cdot\mathbf{v}_g$ and denoting θ the angle between $\mathbf{s}_\alpha$ and $\mathbf{v}_{g,\alpha}$, the element of area $d\sigma_\alpha$ on this surface is

$$d\Omega = \frac{\cos\theta}{s^2} d\sigma_\alpha = \frac{d\sigma_\alpha}{v_{g,\alpha} s_\alpha^3} \tag{28}$$

so

$$\mathbf{G}_+^R(\mathbf{x},\omega) = \frac{i}{8\pi^2}\omega\sum_\alpha \int_{\mathbf{s}\in\Sigma_\alpha} \frac{\mathbf{e}^\alpha}{2v_{g,\alpha}} \mathbf{e}^{i\omega|\mathbf{s}_\alpha\cdot\mathbf{x}|} d\sigma_\alpha. \tag{29}$$

This can be written in a causal form as an integral over forward pointing wave vectors,

$$\mathbf{G}_+^R(\mathbf{x},\omega) = \frac{i}{8\pi^2}\omega\sum_\alpha \int_{\mathbf{s}\in\Sigma_\alpha^+} \frac{\mathbf{e}^\alpha}{v_{g,\alpha}} e^{i\omega\mathbf{s}_\alpha\cdot\mathbf{x}} d\sigma_\alpha. \tag{30}$$

The general result including the anticausal Green's function reads

$$\mathbf{G}_\pm^R(x,y) = \pm i\omega\frac{1}{(2\pi)^2}\sum_\alpha \int_{\mathbf{s}\in\Sigma_\alpha^\pm} d\sigma_\alpha \frac{\mathbf{e}_\alpha}{2v_{g,\alpha}} \mathbf{e}^{i\omega\mathbf{s}\cdot\mathbf{r}}, \tag{31}$$

where $\Sigma_\alpha^\pm$ is the positive or negative of the surface Σ_α, respectively. For the causal Green's function this is to be understood over the upper hemisphere ($s_\parallel > 0$). For the anticausal Green's function, the lower hemisphere is the domain of integration. Furthermore, the group velocity is the opposite of the direction of observation, leading to a sign change of the integrand. In conclusion, the *discontinuity* of the Green's function

FIG. 7. (Color online) Quartz sphere with supporting transducers.

$$\Delta\mathbf{G}(x,y) = \mathbf{G}_+(x,y) - \mathbf{G}_-(x,y) = i\omega\frac{1}{(2\pi)^2}\sum_\alpha \int_{\mathbf{s}\in\Sigma_\alpha} d\sigma_\alpha \frac{\mathbf{e}_\alpha}{2v_{\mathrm{g},\alpha}} \mathbf{e}^{i\omega\mathbf{s}\cdot(\mathbf{x}-\mathbf{y})} \quad (32)$$

is expressed as an integral over the whole slowness surface. Note here the cancellation of the (real) singular part in the discontinuity of the Green's function.

IV. ACCUMULATION OF DATA

In the experiments [16], several shapes were studied. This paper concerns the spectrum of a particular quartz sphere. We shall briefly sketch the experiments; further details will be given in Ref. [16]. The quartz sphere is supported by three transducers; see Fig. 7. The transducers excite the sphere via piezoelectric coupling. The data obtained in the experiment are an arbitrary constant times the complex ratio of the outgoing to the incoming *electric* signal. As the data are complex the actual phase of the response is available. The setup and the measurement techniques are extensions of previous work [10]. The resolution of the setup, characterized by the Q value, is very high. A typical resonance measured in experiment is shown in Fig. 8. Due to the high Q value *ringing* is observed because the transducer frequency changes at a constant rate. The actual position of the single resonance is to the left of the observed peaks as the frequency is swept upwards. Since occasionally two or perhaps even more resonances are close together, the observed signal appears as superpositions of such. The resonances are fitted by using a recognition code [23] which is based on maximum entropy principles. The code fits for each resonance the position in frequency, the decay width, and its (complex) amplitude. It is capable of treating individual resonances with ringing and of superimposing them if they are overlapping. Good performance is observed for the real and imaginary part of the response.

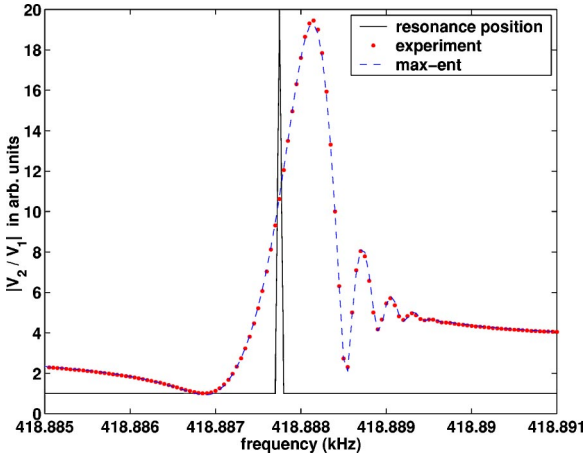

FIG. 8. (Color online) Resonance with ringing due to finite sweep velocity and high Q value.

The quartz sphere was manufactured with a high precision. The spherical shape ensures the discrete symmetry of the crystal, which is described by the symmetry group D_3. However, D_3 is broken to the symmetry group C_3 due to the positions of the transducers in the experiment. Moreover, despite the high precision manufacturing, the shape cannot be perfectly spherical. Its diameter has a relative precision of 5×10^{-5}. At high frequencies this should lead to observable splittings. Finally, gravity leads to an oblate deformation of the sphere. These effects further break the symmetry. Hence the vast majority, if not all, of the symmetry degeneracies are expected to be broken.

V. WEYL CONTRIBUTION

We now discuss the counting function. We work out the leading approximation in Sec. V A and evaluate it numerically in Sec. V B. In Sec. V B, we compare to data obtained in the measurements mentioned in the previous Sec. IV.

A. Approximation to the counting function

The smooth or Weyl part of the level density is the easiest to access. The fluctuations play an important role as well. In fact, the oscillating part of the level density becomes of the same order as the smooth part. Here, however, the focus is on the smooth part. The level density is written formally as

$$d(\omega) = \sum_i \delta(\omega - \omega_i). \quad (33)$$

This can be found from the discontinuity of the Green's function as

$$d(\omega^2) = \frac{1}{2\pi i}\mathrm{Tr}\ \Delta\mathbf{G}(\omega^2) \quad (34)$$

since we here use a Green's function with respect to the squared angular velocity. Now the Green's function is approximated with the corresponding free function. This step is discussed in Ref. [24] and below in this section and corresponds to that in the interior parts of the resonator where the propagation is roughly free. This gives

$$d(\omega^2) = V_x\omega\frac{1}{(2\pi)^3}\sum_\alpha \int_{\mathbf{s}\in\Sigma_\alpha} d\sigma_\alpha \frac{1}{2v_{\mathrm{g},\alpha}}. \quad (35)$$

The volume of the resonator is denoted V_x. The counting function

$$N(\omega) = N(\omega^2) = \int_0^{\omega^2} d(\omega'^2) d\omega'^2 \tag{36}$$

becomes

$$N(\omega) = V_x \frac{\omega^3}{3} \frac{1}{(2\pi)^3} \sum_\alpha \int_{\mathbf{s}\in\Sigma_\alpha} d\sigma_\alpha \frac{1}{v_{g,\alpha}}. \tag{37}$$

From Eq. (21) and geometrical considerations of cones the volume element on a given slowness sheet is

$$dV_\alpha = \frac{1}{3} \frac{d\sigma_\alpha}{v_{g,\alpha}} \tag{38}$$

and therefore

$$N(\omega) = V_x \sum_\alpha V_\alpha \frac{\omega^3}{(2\pi)^3} \tag{39}$$

in terms of the volumes of the slowness sheets, V_α. Somewhat simpler, using frequency f,

$$N(f) = V_x \sum_\alpha V_\alpha f^3. \tag{40}$$

Thus we have a re-derivation of the well-known result: namely, the number of states equals to leading order the available phase space volume.

Although we deal with the anisotropic case, it is instructive to see that the formulas reduce to the result for the isotropic case,

$$N(f) = \frac{4\pi}{3} V_x \left(\frac{1}{c_L^3} + \frac{2}{c_T^3} \right) f^3, \tag{41}$$

where c_L and c_T are the longitudinal and the transverse sound velocities, respectively.

In solid state physics the procedure is different. The resonators are unit cells in crystal lattices. This implies a periodicity assumption of the crystal in contrast to our case of a finite system. Lattice vibrations are connected to the concept of heat and the counting function for vibrations leads to the famous Debye law for the heat capacity. This is derived in Ref. [1].

We will now discuss heuristically why the above derivation is nothing but the leading approximation and correponds to the smooth part of the counting function. Since the trace of the Green's function is taken, it is mainly the local propagation between nearby points which is probed. However, also the possibility of propagation via reflections from the boundary remains. Contributions here come from periodic orbits p but are typically of lesser magnitude than the direct zero length contribution. Ultimately such terms lead to oscillatory contributions to the spectral density. Thus expanding around periodic orbits using the method of stationary phase leads to terms of the form of amplitudes A_p times phases,

$$A_p \exp(i\omega T_p + \cdots), \tag{42}$$

where the (dimensionless) classical action $kL_p = \omega T_p$ in terms of the length/period of the orbit controls the phase of the fluctuations. Averaged over a sufficently large frequency interval the fluctuations dissappear and what remains is the part from zero length orbits. The latter do not fluctuate and represents the average contribution.

TABLE I. Elastic constants for quartz at room temperature.

Units	C11	C12	C13	C14	C33	C44
10^{11} N/m^2	0.868	0.0704	0.1191	−0.1804	1.0575	0.5820

B. Numerical calculation and prediction

At room temperature $T_r = 22°$C, the mass density is $\rho = 2.6485$ g/cm^3, and the diameter of the sphere measures 87.75 mm. The elastic constants for quartz at room temperature are listed in Table I.

They are given in Voigt notation. Pairs of Cartesian indices ij with $i,j \in \{x,y,z\}$ are numbered as follows: $xx=1$, $yy=2$, $zz=3$, $yz=4$, $zx=5$, and $xy=6$. Thus, for example, c_{xxyz} is denoted C14.

We now calculate the leading Weyl term (40). The volume in slowness space is conveniently expressed as an integral over the unit sphere,

$$V_s = \sum_\alpha V_\alpha = \sum_\alpha \frac{1}{3} \int_{\mathbf{n}\in S^2} s_\alpha^3 d\mathbf{n}. \tag{43}$$

The three lengths of the slowness vectors are found from Eqs. (10) and (11). In particular, the squares of the velocities are found from Eqs. (25) and (26). Therefore Eq. (43) reduces to

$$V_s = \frac{1}{3} \int_{\mathbf{n}\in S^2} \mathrm{tr}(\mathbf{\Gamma}(\mathbf{n})^{-3/2}) d\mathbf{n}, \tag{44}$$

which is easily calculated from the eigenvalues of $\mathbf{\Gamma}(\mathbf{n})$. Finally the symmetry can be exploited: In the case of quartz it is enough to integrate over a fundamental region $0 \leqslant \phi \leqslant 2\pi/3$ and $0 \leqslant \theta \leqslant \pi/2$ and multiply by 6. Using the elastic constants in Table I, we find the volume in slowness space by numerical integration,

$$V_s = 1.4909 \times 10^{-10} (\mathrm{sec/m})^3. \tag{45}$$

This volume may be used for various shapes of resonators upon multiplication with the particular volumes in physical x space. Hence, combining everything, the number of states for our sphere should grow as

$$N(f) = Af^3 + O(f^2) \tag{46}$$

with the constant

$$A = 5.274 \times 10^{-14} \mathrm{sec}^3 \tag{47}$$

as the result of our computation.

The elastic constants change with temperature. In Appendix B, they are given in terms of an expansion. As the experiment was performed at $T = 30°$C, we also calculate the volumes in slowness space with these corrected constants. However, it turns out that the relative difference to the calculation for room temperature is of the order of 10^{-8}, that is, within the numerical errors. Similarly, the temperature de-

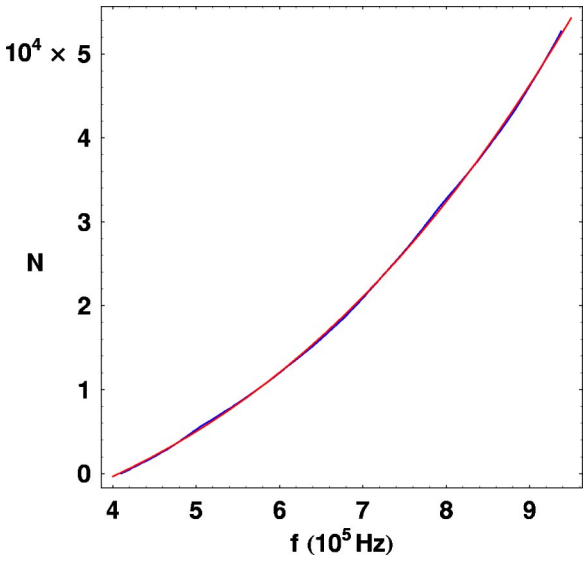

FIG. 9. (Color online) Spectral staircase: experiment and fit.

pendence of the mass density, see Appendix B, has no influence either.

C. Comparing with experiment

The spectrum used here was measured from 410 to 960 KHz. The resonances were identified by means of the recognition routine [23]; mentioned in Sec. IV. Roughly 52 000 resonances were found. Here the bulk term in Eq. (46) contributes with at least 43 000 resonances. The staircase for the experiment is fitted with a cubic polynomial; see Fig. 9. For the leading coefficient we find

$$A_{\text{fit}} = 5.030 \times 10^{-14}\text{sec}^3. \tag{48}$$

This is in good agreement with the theoretical result (47). The relative error is 4.6%.

The difference between the fitted and the experimental counting function is plotted in Fig. 10. The sizable deviation between fit and experiment is striking. It resembles a sawtooth with very rapid fluctuations on top. We Fourier transform this oscillating structure and obtain the period spectrum; see Fig. 11. From this we estimate the time

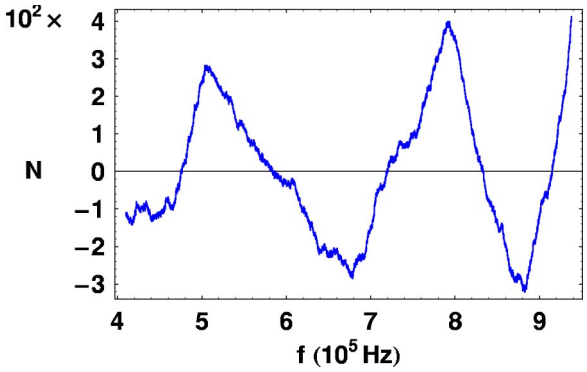

FIG. 10. (Color online) Fluctuations of the counting function.

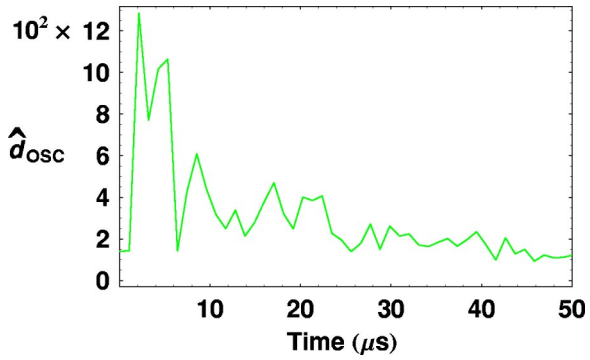

FIG. 11. (Color online) Period spectrum.

corresponding to the largest peak to approximately 2 μsec. Also other peaks at $4, 9, 13, 17, 20, \ldots$ μsec are observed. As the frequency interval sampled is approximately 500 KHz the resolution is roughly 2 μsec. It is tempting to interpret the largest peak as due to the shortest bouncing-ball-type mode, that is, a wave packet bouncing back and forth along some diameter of the sphere. If we take the velocities to lie between 5 and 10 km/sec the shortest period is around 17.8 μsec. Therefore the peak corresponding to the sawtooth oscillations is not likely to be due to such a mode and remains unexplained so far. Likewise the remaining short times less than the estimate 17.8 μsec are not explained.

VI. SUMMARY AND CONCLUSION

We have discussed the experimental spectrum of a quartz sphere from the point of view of the spectral counting function. The classical phase space volume gives indeed the leading behavior of this object. On calculating this numerically we find it in good agreement with the experimentally fitted term. This paves the way for further studies of elastic spectra, such as boundary corrections to the counting function [25,26] and periodic orbit theory for the fluctuations in the level density [13–15].

Due to the boundary further resonances should be present. Less is not expected as the boundary conditions allow for surface waves in analogy with Neumann conditions for the Helmholtz case. It is currently an open problem to incorporate this surface contribution in the anisotropic case. Nevertheless, such surface modes couple to the bulk and are not exponentially damped in this elastic case. Therefore experiments should access these states and thereby the surface correction to the leading volume term as well.

The fluctuating part would involve recent semiclassical methods. Here individual closed rays, periodic orbits, control the oscillations in the level density. In particular this has been shown not just for quantum mechanical spectra but also more recent in two dimensional elastodynamic resonators. The step to three dimensions plus anisotropy has yet to be made.

ACKNOWLEDGMENTS

N.S. and T.G. acknowledge discussions with S. Creagh and J.D. Achenbach and financial support from the Rosen-

feld Foundation, the Crafoord Foundation, and from Det Svenska Vetenskapsrådet, respectively. M.O. thanks the Division of Mathematical Physics, LTH, for hospitality during his visits to Lund.

APPENDIX A: RADON TRANSFORM AND THE GREEN's FUNCTION

Following Ref. [21] we first solve the Radon transformed time problem. Next the solution is transformed back, and finally Fourier transforming gives the frequency dependent Green's function.

Radon transform

The equation $s=\mathbf{n}\cdot\mathbf{x}$ describes a plane with the normal vector $\mathbf{n}$ in the space of the position vector $\mathbf{x}$. The plane cuts the direction defined by $\mathbf{n}$ in the height s. The Radon transform $\hat{f}(s,\mathbf{n})$ of a function $f(\mathbf{x})$ is the average

$$\mathcal{R}f(s,\mathbf{n})=\hat{f}(s,\mathbf{n})=\int f(\mathbf{x})\delta(s-\mathbf{n}\cdot\mathbf{x})d\mathbf{x} \tag{A1}$$

over the plane for a given height s. The Radon transform of the spatial derivatives of the function $f(\mathbf{x})$ fulfills

$$\mathcal{R}\left(\frac{\partial f}{\partial x^i}\right)(s,\mathbf{n})=n_i(\partial_s\mathcal{R}f)(s,\mathbf{n}). \tag{A2}$$

We now apply this to the time dependent elastic problem (1). We denote the Green's function $\mathbf{G}(\mathbf{x},t)$ and its Radon transform $\hat{\mathbf{G}}(s,\mathbf{n})$. We find

$$[\mathbf{\Gamma}(\mathbf{n})\partial_s^2-1\partial_t^2]\cdot\hat{\mathbf{G}}=-1\delta(s)\delta(t), \tag{A3}$$

where the matrix $\mathbf{\Gamma}$ is defined in Eqs. (25) and (26). We observe that $\hat{\mathbf{G}}(s,\mathbf{n})$ also depends on time t. The initial condition is taken as causal such that $\hat{\mathbf{G}}(s,\mathbf{n})=0$ for $t<0$. Necessary and sufficient conditions for solving this problem are found by projecting onto the subspaces defined by the individual polarizations:

$$(c_\alpha^2\partial_s^2-\partial_t^2)\mathbf{e}^\alpha\cdot\hat{\mathbf{G}}(\mathbf{s},\mathbf{n})=-\mathbf{e}^\alpha\delta(s)\delta(t), \tag{A4}$$

where c_α is the phase velocity associated with polarization α and $\mathbf{e}^\alpha$ is the corresponding projector. Invoking d'Alembert's solution

$$\mathbf{e}^\alpha\cdot\hat{\mathbf{G}}(s,\mathbf{n})=\mathbf{e}^\alpha\frac{H(t)}{2c_\alpha}[H(s+c_\alpha t)-H(s-c_\alpha t)] \tag{A5}$$

with H the Heaviside unit step function, we find

$$\hat{\mathbf{G}}(s,\mathbf{n})=\sum_\alpha\mathbf{e}^\alpha\frac{H(t)}{2c_\alpha}[H(s+c_\alpha t)-H(s-c_\alpha t)], \tag{A6}$$

which is the full solution.

Inverse Radon transform

The inverse Radon transform is given by

$$f(\mathbf{x})=-\frac{1}{8\pi^2}\int_{\mathbf{n}\in S^2}d\Omega\ \left.\frac{d^2(\mathcal{R}f)(s,\mathbf{n})}{ds^2}\right|_{s=\mathbf{n}\cdot\mathbf{x}} \tag{A7}$$

following from the identity

$$\delta(\mathbf{x})=-\frac{1}{8\pi^2}\int_{\mathbf{n}\in S^2}d\Omega\,\delta''(\mathbf{n}\cdot\mathbf{x}). \tag{A8}$$

The latter is proved using

$$2\pi|\mathbf{x}|=\int_{\mathbf{n}\in S^2}d\Omega|\mathbf{n}\cdot\mathbf{x}|$$

and the identities $|x|=2\delta(x)$, $\Delta(1/|\mathbf{x}|)=-4\pi\delta(\mathbf{x})$ and $\Delta|\mathbf{x}|=2/|\mathbf{x}|$. Hence we find the Green's function in configuration space,

$$\begin{aligned}\mathbf{G}(\mathbf{x},t)&=-\frac{H(t)}{16\pi^2}\int_{\mathbf{n}\in S^2}d\Omega\sum_\alpha\frac{\mathbf{e}^\alpha}{c_\alpha^2}\partial_t[\delta(c_\alpha t+\mathbf{n}\cdot\mathbf{x})\\&\quad+\delta(c_\alpha t-\mathbf{n}\cdot\mathbf{x})]\\&=-\frac{H(t)}{8\pi^2}\int_{\mathbf{n}\in S^2}d\Omega\sum_\alpha\frac{\mathbf{e}^\alpha}{c_\alpha^2}\partial_t\delta(c_\alpha t-\mathbf{n}\cdot\mathbf{x}),\end{aligned} \tag{A9}$$

by inverting Eq. (A6).

Frequency domain

The frequency dependent Green's function $\mathbf{G}(x,\omega)$ is obtained by Fourier transforming Eq. (A9) with respect to time:

$$\begin{aligned}\mathbf{G}(\mathbf{x},\omega)&=-\frac{1}{8\pi^2}\int_{\mathbf{n}\in S^2}d\Omega\sum_\alpha\frac{\mathbf{e}^\alpha}{c_\alpha^2}\int_{-\infty}^{\infty}dte^{i\omega t}H(t)\partial_t\\&\quad\times\delta(c_\alpha t-\mathbf{n}\cdot\mathbf{x}).\end{aligned} \tag{A10}$$

The inner integral is found by partial integration: the time derivative will act either on the exponential or the step function leading to the regular respective singular contribution

$$\begin{aligned}\mathbf{G}_+^R(\mathbf{x},\omega)&=\frac{i}{8\pi^2}\int_{\mathbf{n}\cdot\mathbf{x}>0}\sum_\alpha\frac{k_\alpha\mathbf{e}^\alpha}{c_\alpha^2}e^{ik_\alpha\mathbf{n}\cdot\mathbf{x}}d\Omega\\&=\frac{i}{8\pi^2}\int_{\mathbf{n}\in\mathbf{S}^2}\sum_\alpha\frac{k_\alpha\mathbf{e}^\alpha}{2c_\alpha^2}\mathbf{e}^{ik_\alpha|\mathbf{n}\cdot\mathbf{x}|}d\Omega\end{aligned} \tag{A11}$$

and

$$\mathbf{G}^S(\mathbf{x},\omega)=\frac{1}{8\pi^2}\int_{\mathbf{n}\in S^2}\mathbf{\Gamma}^{-1}(\mathbf{n})\delta(\mathbf{n}\cdot\mathbf{x})d\Omega.$$

The anticausal Green's function is found similarly by reversing the time in, say, Eq. (A6). In particular, the same singular part is otained whereas the regular part is the complex conjugate of the causal regular part.

APPENDIX B: TEMPERATURE DEPENDENCE

The resonator is kept at fixed temperature

$$T=30\ ^\circ\mathrm{C} \tag{B1}$$

with a precision on the order of a mK. This is slightly higher than the room temperature $T_r=22\,^\circ$C, at which the quartz

TABLE II. Coefficients of temperature expansion for elastic constants of quartz.

Order	Units	C11	C12	C13	C14	C33	C44
0	10^{11} N/m^2	0.868	0.0704	0.1191	−0.1804	1.0575	0.5820
1	10^{-6}/K	−48.5	−3000	−550	101	−160	−177
2	10^{-9}/K^2	−107	−3050	−1150	−48	−275	−216
3	10^{-12}/K^3	−70	−1260	−750	−590	−250	−216

TABLE III. Coefficients for the temperature expansion of the mass density of quartz.

Order	Units	ρ
0	10^3kg/m^3	2.6485
1	10^{-6}/K	−34.80
2	10^{-9}/K^2	−30.04
3	10^{-12}/K^3	49.08

sphere was manufactured. This causes a change in the elastic constants described below in terms of a power series expansion around room temperature,

$$c_{ijkl}(T) = c_{ijkl,0} + c_{ijkl,1}(T - T_r) + c_{ijkl,2}(T - T_r)^2 + c_{ijkl,3}(T - T_r)^3 + \cdots . \quad \text{(B2)}$$

We took the coefficients of this expansion from Ref. [27]; they are listed in Table II.

Furthermore, a change in mass density takes place. In Table III, we list the coefficients of an expansion around room temperature.

Finally, there is also a shape deformation, expressed in terms of the tensor of thermal expansion according to $u_i' = \alpha_{ij} u_j$.

The effect of temperature change is therefore mainly to change the shape and volume of the k part of the available phase space volume, namely the slowness surface. Thus the first table is most important for our purposes. We have calculated the new volume in slowness space at the corresponding experimental temperature to cubic order in the temperature change. The other, relative changes turn out to be negligible, namely of the order 10^{-8}.

[1] N. W. Ashcroft and N. D. Mermin, *Solid State Physics* (Holt, Rinehart and Winston, New York, 1976).

[2] P. Cvitanović, R. Artuso, R. Mainieri, and G. Vattay, *Classical and Quantum Chaos* (Niels Bohr Institute, Copenhagen, 2002), www.nbi.dk/ChaosBook/

[3] M. C. Gutzwiller, *Chaos in Classical and Quantum Mechanics* (Springer, New York, 1990).

[4] M. Brack and R. K. Bhaduri, *Semiclassical Physics* (Addison-Wesley, Reading, MA, 1997).

[5] H.-J. Stöckmann, *Quantum Chaos: An Introduction* (Cambridge University Press, Cambridge, England, 1999).

[6] H. P. Baltes and E. R. Hilf, *Specta of Finite Systems* (Bibliographisches Institut, Mannheim, 1976).

[7] F. Faure and B. Zhilinskii, Phys. Lett. A **302**, 242 (2002).

[8] R. L. Weaver, J. Acoust. Soc. Am. **85**, 1005 (1989).

[9] C. Ellegaard, T. Guhr, K. Lindemann, H. Q. Lorensen, J. Nygård, and M. Oxborrow, Phys. Rev. Lett. **75**, 1546 (1995).

[10] C. Ellegaard, T. Guhr, K. Lindemann, J. Nygård, and M. Oxborrow, Phys. Rev. Lett. **77**, 4918 (1996).

[11] P. Bertelsen, C. Ellegaard, T. Guhr, M. Oxborrow, and K. Schaadt, Phys. Rev. Lett. **83**, 2171 (1999).

[12] K. Schaadt, T. Guhr, C. Ellegaard, and M. Oxborrow, Phys. Rev. E **68**, 036205 (2003).

[13] L. Couchman, E. Ott, and T. M. Antonsen Jr., Phys. Rev. A **46**, 6193 (1992).

[14] N. Søndergaard and G. Tanner, Phys. Rev. E **66**, 066211 (2002).

[15] E. Bogomolny and E. Hugues, Phys. Rev. E **57**, 5404 (1998).

[16] M. Oxborrow, C. Ellegaard, and K. Schaadt (unpublished).

[17] A. N. Cleland, *Foundations of Nanomechanics* (Springer, Berlin, 2002).

[18] L. D. Landau and E. M. Lifshitz, *Theory of Elasticity* (Pergamon, Oxford, 1959)

[19] B. A. Auld, *Acoustic Fields and Waves in Solids I, II* (Wiley, New York, 1973).

[20] M. J. P. Musgrave, *Crystal Acoustics* (Holden-Day, San Francisco, 1970).

[21] C. Y. Wang, A. Saez, and J. D. Achenbach, *3-D Elastodynamic Green's Functions for BEM Applications to Anisotropic Solids*, IUTAM Symposium on Anisotropy, Inhomogeneity and Nonlinearity in Solid Mechanics, edited by D. F. Parker and A. H. England, 1995, p. 307.

[22] R. Burridge, Q. J. Mech. Appl. Math. **20**, 41 (1967).

[23] M. Oxborrow (unpublished).

[24] R. Balian and C. Bloch, Ann. Phys. (N.Y.) **60**, 401 (1970).

[25] M. Dupuis, R. Mazo, and L. Onsager, J. Chem. Phys. **33**, 1452 (1960).

[26] Y. Safarov and D. Vassiliev, in *Spectral Theory of Operators*, edited by S. Gindikin, AMS Translations Ser. 2, 1992, Vol. 150.

[27] R. Bechmann, Phys. Rev. **110**, 1060 (1958).